Vol. 80 (1991) *ACTA PHYSICA POLONICA A* No 2

Proceedings of the XX International School of Semiconducting Compounds, Jaszowiec 1991

PHYSICS OF SOLID-STATE LASER MATERIALS*

A.J. WOJTOWICZ

Institute of Physics, N. Copernicus University, ul. Grudziądzka 5, 87–100 Toruń, Poland and Chemistry Department, Boston University 590 Commonwealth Ave., Boston, 02215 MA, USA

A survey of the physical properties of solid state materials activated with d^2, d^3 and d^8 transition metal ions is presented in the context of tunable laser operation. An emphasis is put on common characteristics of all three systems, like a strong electron–phonon coupling and similar electronic structures. The conditions necessary to obtain a tunable operation and to avoid an overlap of the excited state absorption and emission are formulated. It is shown that the d^3 configuration system has the largest range of allowed values of the crystal field parameter $10Dq$.

PACS numbers: 42.55Rz, 78.50.–w 78.55.–m

1. Introduction

Solid-state lasers are nowadays broadly used in a variety of industrial, medical and military applications. The largest share of the laser market belongs to Nd lasers (glass and YAG) and CO_2 lasers which are widely used for cutting, drilling and welding by materials processing industries. The largest lasers, developed for the laser-driven fusion, are again Nd lasers based on glass. On the other hand the compactness of the (low energy) solid-state lasers makes them strong contenders in the field of military applications (range finders and target designators) while wavelength tunability and high peak power point to applications like a laser isotope separation or versatile light sources driven by flashlamps, semiconductor laser arrays, e-beam pumped phosphors or cw gas lasers. High-power, single-wavelength, Nd lasers operating in the infrared and coupled to efficient harmonic sources may be used to drive optical parametric oscillators or other tunable solid-state lasers to further extend the spectral range covered. Therefore it seems that the development of better laser materials based on new ions and/or hosts to meet diversified requirements of new and demanding applications is highly desirable [1].

*This work is based on the program supported by the Grant No. DAAL03-86-K-0016 of the US Army Research Office.

In this paper we will concentrate on some aspects of one particular class of tunable solid-state lasers based on transition metal (TM) ions. Stimulated emission cross-sections, tunability, excited state absorption (ESA), laser level lifetime and non-radiative transitions competing for the excited state population are the most important factors for performance of the laser. The characteristics of the given ion-host combination are determined by the electronic structure of the TM ion in a particular host. This includes electronic states, their spin and symmetry properties, and interactions, like an electron–lattice and spin–orbit couplings. What we aim at in this paper, is to give a simple but comprehensive picture of the physics involved in the performance of this particular type of laser. We will concentrate on the consequences of the coupling to the lattice and electronic structure of the TM ion on the performance of the laser with emphasis on tunability and ESA. We will develop a simple approach, based on the ligand field theory, to classify and characterize different laser materials. Although in the scheme we shall present, there still is a considerable amount of unpredictibility, some generally observed trends, like the success of the Cr^{3+}-doped materials, are, at least qualitatively, explained.

2. Tunable solid-state laser materials

Good materials for tunable solid state lasers based on TM ions should fulfill following conditions (see also [2]):

a) broad, spin-allowed bands in absorption matching the spectrum of the Xe flashlamps,

b) broad, efficient and spin-allowed emission to achieve flexible wavelength tunability in hosts characterized by the appropriate value of the 10 Dq parameter,

c) emission decay times matching the decay times of Xe flashlamps,

d) resistance to both oxidation and reduction (one charge state),

e) possibly large stabilization energy in the octahedral crystal field,

f) the gap in the excited state absorption (ESA) at the emission wavelengths.

In requirements listed above, the efficient pumping by Xe flashlamps was included although it is not always possible and even desirable. In many cases pumping by gas lasers or laser diode arrays is preferable. However, pumping with Xe flashlamps is now the only practical way to achieve high peak power.

In the next paragraph we will consider the coupling of the TM ion to the lattice, responsible for the broad emission and absorption bands. Then the electronic structure of the TM ion itself will be discussed with emphasis on some of the requirements listed above.

3. The TM ion and the lattice

To describe the system consisting of the TM ion with n d-electrons and the lattice it is a common practice to resort to some generally accepted approximations:

1) d-electrons move and interact with each other in the slowly changing field generated by inner shell electrons and nuclei of the metal ion and ligands ("adiabatic" or Born–Oppenheimer approximation), and

2) the lattice can be approximated by a set of independent harmonic oscillators representing different vibrational modes (harmonic approximation).

We postpone a discussion of the TM ion electronic problem to the next paragraph. For now we assume that we already know electronic energies $E_\mu(Q_0)$ and wave functions $\phi_\mu(q, Q_0)$ of the static problem:

$$H_{\mathrm{el}}(q, Q_0)\phi_\mu(q, Q_0) = E_\mu(Q_0)\phi_\mu(q, Q_0), \tag{1}$$

where

$$H_{\mathrm{el}}(q, Q_0) = \sum_{i=1}^{n}\left[\frac{\hbar^2}{2m}\nabla_{q_i}^2 + V_{\mathrm{el}}(q_i, Q_0)\right] + \sum_{i>j=1}^{n}\frac{e^2}{q_{ij}} + H_{\mathrm{s-o}}(q) \tag{2}$$

is the electronic Hamiltonian for the lattice frozen at some position Q_0. Electronic energies and wave functions can be then improved by incorporation of the electron–lattice term:

$$H_{\mathrm{el-ph}}(Q - Q_0) = \sum_{j=1}^{N}(Q_j - Q_0)\sum_{i=1}^{n}\frac{\partial}{\partial Q_j}V_{\mathrm{el}}(q_i, Q)|_{Q=Q_0} \tag{3}$$

using e.g. perturbation theory or diagonalization of the $H_{\mathrm{el}} + H_{\mathrm{el-ph}}$ Hamiltonian. In (3), $V_{\mathrm{el}}(q_i, Q)$ is the instantaneous potential seen by the i-th electron. Since only local modes of lattice vibrations will couple effectively to localized optical transitions on the TM ion, N can be reasonably limited e.g. to 21 symmetry modes for the O_h symmetry (when only six nearest neighbors and the TM ion itself are included). Let us note that for the full symmetry lattice mode A_{1g} dominating in (3):

$$\langle\phi_\mu(q, Q_0)|H_{\mathrm{el-ph}}(Q - Q_0)|\phi_\nu(q, Q_0)\rangle \begin{cases} = 0 & \text{for } \mu \neq \nu \\ \neq 0 & \text{for } \mu = \nu \end{cases} \tag{4}$$

which means that the full symmetry A_{1g} distortion changes energies but does not mix different electronic states. The reason is that the integrand in (4) will transform like the Kronecker product representation $\Gamma_\mu \times \Gamma \times \Gamma_\nu$ where Γ is a representation of some vibrational mode. The integral will not be equal to zero only when reduction of the $\Gamma_\mu \times \Gamma \times \Gamma\nu$ representation yields a term A_{1g}. For $\Gamma = A_{1g}$, $\Gamma_\mu \times \Gamma_\nu$ has to be equal to A_{1g} which happens only for $\mu = \nu$. In some cases the electron–lattice term for low symmetry vibrations can be very important

(for the review of the Jahn–Teller effect see [3]). As long as this is not the case the inclusion of the electron–lattice coupling yields improved energies:

$$E_\mu(Q) = E_\mu(Q_0) + V_{\mu\mu}(Q_{A_{1g}} - Q_0), \tag{5}$$

where $V_{\mu\mu} = \langle\phi_\mu(q, Q_0)|\partial V_{\mathrm{el}}(q, Q)/\partial Q_{A_{1g}}|_{Q=Q_0}|\phi_\mu(q, Q_0)\rangle$ may assume different values for different electronic states. The consequences of this fact as well as the problem of the spin–orbit term H_{s-o} are discussed elsewhere [4].

The next step is to find solutions of the total Hamiltonian, including lattice. It can be shown that these solutions can be approximated by the following wave functions:

$$\phi_{\mu i}(q, Q) = \phi_\mu(q, Q_0)\chi_i(Q), \tag{6}$$

where $\chi_i(Q)$ constitute solutions of the equation:

$$\left(\sum_{j=1}^{N} \frac{\hbar^2}{2M}\nabla^2_{Q_j} + V_{\mathrm{ion}}(Q) + E_\mu(Q_0) + V_{\mu\mu}(Q_{A_{1g}} - Q_0)\chi_i(Q)\right) =$$
$$= E_{\mu i}\chi_i(Q). \tag{7}$$

In (7) the electronic part of the total Hamiltonian was simply substituted by its solution (5) and $V_{\mathrm{ion}}(Q)$ stands for the lattice potential energy term.

To find energies $E_{\mu i}$, corresponding to $|\mu i\rangle$ states represented by (6), the next approximation, so-called harmonic approximation, is usually adopted. The idea is to subsitute $V_{\mathrm{ion}}(Q)$ in equation (7) with the harmonic oscillator potential. Then:

$$\left[\sum_{j=1}^{N}\left(\frac{\hbar^2}{2M_j}\nabla^2_{Q_j} + \frac{1}{2}M_j\omega_j^2Q_j^2\right) + E_\mu(Q_0) + V_{\mu\mu}(Q_{A_{1g}} - Q_0\chi_i(Q)\right] =$$
$$= E_{\mu i}\chi_i(Q), \tag{8}$$

where M_j is the effective mass and ω_j is the frequency of the j-th normal mode. The adiabatic potential $V^\mu_{\mathrm{ad}}(Q)$:

$$V^\mu_{\mathrm{ad}}(Q) = E_\mu(Q_0) + V_{\mu\mu}(Q_{A_{1g}} - Q_0) + \frac{1}{2}\sum_{j=1}^{N} M_j\omega_j^2Q_j^2 \tag{9}$$

serves as a harmonic oscillator potential with a new equilibrium position determined by a term linear in Q. If we choose Q_0 at the equilibrium position of the lattice in the ground electronic state, (say, $\mu = g$), and assume that the electronic energy in this state $E_g(Q_0) = 0$, we will have:

$$V^g_{\mathrm{ad}}(Q) + \frac{1}{2}M_{A_{1g}}\omega^2_{A_{1g}}(Q_{A_{1g}} - Q_0)^2, \tag{10}$$

and for the first excited state (say $\mu = \mathrm{e}$):

$$V^{\mathrm{e}}_{\mathrm{ad}}(Q) = \frac{1}{2}M_{A_{1g}}\omega^2_{A_{1g}}(Q_{A_{1g}} - Q^{\mathrm{e}}_0)^2 + E_{\mathrm{e}}(Q_0) - \frac{1}{2}\frac{V^2_{\mathrm{ee}}}{M_{A_{1g}}\omega^2_{A_{1g}}}. \tag{11}$$

$E_e(Q_0)$ is the electronic energy and Q_0^e is the new equilibrium position in the first excited state:

$$Q_0^e = Q_0 - \frac{V_{ee}}{M_{A_{1g}}\omega_{A_{1g}}^2}. \tag{12}$$

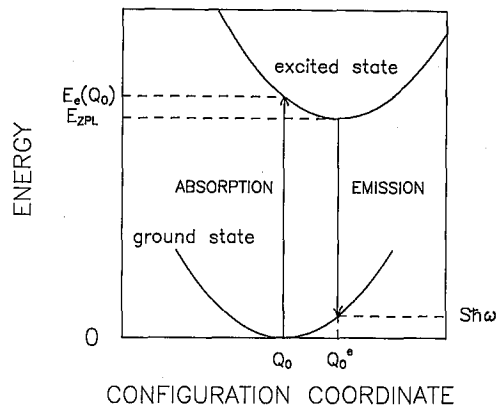

Fig. 1. Configuration coordinate diagram of the TM ion in the solid state matrix. The total potential energy of the ion-lattice system in the ground and excited states is shown vs. a configurational coordinate representing a full symmetry lattice distortion around the TM ion. Vertical arrows designate absorption and emission transitions. Excited state electronic energy at equilibrium position of the lattice and energy of the zero-phonon sharp line transition are indicated. The lattice relaxation energy is $S\hbar\omega$.

The energy of the zero-phonon line E_{ZPL} (see Fig. 1) will be:

$$E_{ZPL} = E_e(Q_0) - \frac{1}{2}\frac{V_{ee}^2}{M_{A_{1g}}\omega_{A_{1g}}^2}. \tag{13}$$

In (10) and (11) the contributions from all the other vibrations modes (except the full symmetry mode A_{1g}), which do not couple to the electronic transitions (hence contribute the same energies to the $E_{\mu i}$ for every μ which then cancel in the transition), were omitted. In this approximation the lattice relaxation energies in the excited state (after absorption) and in the ground state (after emission) are the same and equal to $S\hbar\omega_{A_{1g}}$ (S is the Huang–Rhys parameter). Therefore $2S\hbar\omega_{A_{1g}}$ corresponds to the difference in energy between peaks of the absorption and emission bands (the Stokes shift). The relation between experimentally accessible $S\hbar\omega_{A_{1g}}$ and the electron–phonon coupling matrix element V_{ee} for the first excited state $|e\rangle$ is:

$$S\hbar\omega_{A_{1g}} = \frac{1}{2}\frac{V_{ee}^2}{M_{A_{1g}}\omega_{A_{1g}}^2}. \tag{14}$$

In this approximation the total energy of the $|\mu, i\rangle$ state is:

$$E_{\mu i} + E_{\mu}(Q_0) - \frac{1}{2}\frac{V_{\mu\mu}^2}{M_{A_{1g}}\omega_{A_{1g}}^2} + (i + \frac{1}{2})\hbar\omega_{A_{1g}}, \tag{15}$$

and functions $\chi_i(Q)$ are simply the harmonic oscillator wave functions.

The Stokes shift and broadness of absorption and emission bands are consequences of the electron–lattice coupling as described above. Broad bands in absorption are instrumental for the efficient coupling of the broad band pumping light source to the laser material, whereas broad band in emission is necessary for the tunability. Strong (or intermediate) coupling to the lattice of absorption and emission transitions is therefore a necessary condition which tunable laser material should fulfill (see requirements a) and b) in the previous paragraph). The reasons why some states do couple strongly to the lattice and some do not will be given in the next paragraph.

4. The electronic structure of the TM ion

In this paragraph we will consider the electronic structure of the TM ion. In the strong field approximation the zero-order electronic Hamiltonian:

$$H_{\mathrm{el}}^0(q, Q_0) = \sum_{i=1}^{n}\left[\frac{\hbar^2}{2m}\nabla_{q_i}^2 + V_{\mathrm{el}}(q_i, Q_0)\right], \tag{16}$$

consists of n one-electron Hamiltonians, which can be solved separately. The electron–electron Coulumb interaction term will be included later. In the octahedral crystal field potential $V_{\mathrm{el}}(q_i, Q_o)$ transforms like the A_{1g} representation of the O_h group and the fivefold degenerate $l = 2$ representation spanned by one-electron d-functions reduced to $t_{2g} + e_g$. Since reduction of $t_{2g} \times t_{2g}$ and $e_g \times e_g$ does yield A_{1g} while for $t_{2g} \times e_g$ it does not, the d-level of the TM ion splits into two levels, designated e_g and t_{2g}. The energy difference between these levels defines the so-called crystal field parameter $10Dq$:

$$\langle e_g|V_e(q_i, Q_0)|e_g\rangle - \langle t_{2g}|V_e(q_i, Q_0)|t_{2g}\rangle = 10Dq \tag{17}$$

which relates to the strength of the crystal field generated by ligands and usually is taken from the experiment. The total electronic energy of the system consisting of $n + m$ electrons in the $t_{2g}^n e_g^m$ strong field configuration is, in this approximation, given by $-E_{\mathrm{stab}} = (6m - 4n)Dq$ and its wave function can be represented by a Slater determinant built from the n one-electron t_{2g} wave functions and m one-electron e_g wave functions. The positive, or equal zero energy E_{stab} assumes maximum value of $12Dq$ for d^3 and d^8 configurations and $8Dq$ for d^2 and d^7 configurations. These four configurations cover all the TM ions which were demonstrated to lase (Cr^{3+}, V^{2+}, Ni^{2+} and Co^{2+}) with only one exception of Ti^{3+} [2, 5]. Assuming that the energy of the ground state configuration is zero, the consecutive higher energy configurations will have zero-order energies $10Dq$, $20Dq$, $30Dq$. According to the perturbation theory the high degeneracy of every configuration will

be partially removed and improved energies and wave functions will be obtained by diagonalization of the total Hamiltonian including the electron–electron Coulomb interaction in the appropriate basis [6, 7]. Since this interaction transforms like the A_{1g} representation of the O_h group, matrix elements $\langle \Gamma_\mu | \sum_{i>j=1}^{n} e^2/q_{ij} | \Gamma_\nu \langle$ will transform like $\Gamma_\mu \times \Gamma_\nu \times A_{1g}$ where $|\Gamma_\mu\rangle$ and $|\Gamma_\nu\rangle$ designate many-electron states described by wave functions transforming like Γ_μ and Γ_ν representations of the O_h symmetry group. These matrix elements will be equal to zero in all cases except when $\mu = \nu$. In other words, the electron–electron Coulomb interaction will change the energy of each term Γ_μ (diagonal matrix elements) but non-diagonal matrix elements will be different from zero only for the terms of the same symmetry coming from different strong field configurations. If $10Dq$ is much larger than electrostatic splittings in the configuration than it is resonable to omit non-diagonal matrix elements.

TABLE I

Energies of selected electronic states of the d^2 configuration.

Conf.	State	Energy	Characteristic of the transition state to given state	
			lattice coupling	oscillator strength
t_{2g}^2	$^3T_{1g}$	$-5B$		
	^1E_g	$B+2C$	weak	weak
	$^1T_{2g}$	$B+2C$	weak	weak
	$^1A_{1g}$	$10B+5C$	weak	weak
$t_{2g}e_g$	$^3T_{2g}$	$10Dq-8B$	strong	strong
	$^3T_{1g}$	$10Dq+4B$	strong	strong
e_g^2	$^3A_{2g}$	$20Dq-8B$	very strong	weak

TABLE II

Energies of selected electronic states of the d^3 configuration.

Conf.	State	Energy	Characteristic of the transition state to given state	
			lattice coupling	oscillator strength
t_{2g}^3	$^4A_{2g}$	$3A-15B$		
	^2E_g	$3A-6B+3C$	weak	weak
	$^2T_{1g}$	$3A-6B+3C$	weak	weak
	$^2T_{2g}$	$3A+5C$	weak	weak
$t_{2g}^2e_g$	$^4T_{2g}$	$10Dq+3A-15B$	strong	strong
	$^4T_{1g}$	$10Dq+3A-3B$	strong	strong
$t_{2g}e_g^2$	$^4T_{1g}$	$20Dq+3A-12B$	very strong	weak

TABLE III

Energies of selected electronic states of the d^8 configuration.

Conf.	State	Energy	Characteristic of the transition state to given state	
			lattice coupling	oscillator strength
$t_{2g}^6 e_g^2$	$^3A_{2g}$	$-8B$		
	^1E_g	$2C$	weak	weak
	$^1A_{1g}$	$8B+4C$	weak	weak
$t_{2g}^5 e_g^3$	$^3T_{2g}$	$10Dq-8B$	strong	strong
	$^3T_{1g}$	$10Dq+4B$	strong	strong
$t_{2g}^4 e_g^4$	$^3T_{1g}$	$20Dq-5B$	very strong	weak

In Tables I to III we present energies of selected electronic states of d^2, d^3 and d^8 configurations within this approximation based on Coulomb interaction matrices published in [6]. The reason for choosing these three configurations is the striking similarity of their electronic structures (see Fig. 2). Unfortunately the d^1

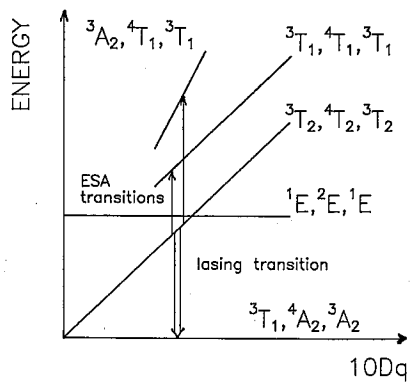

Fig. 2. Tanabe–Sugano diagram. The energies of electronic states of different strong field configurations are shown vs. crystal field parameter $10Dq$. Horizontal lines indicate states of the lowest energy configuration, slope one lines are due to the next configuration ($10Dq$) and slope two line comes from the $20Dq$ strong field configuration. Electronic states belonging to d^2, d^3 and d^8 configurations are listed consecutively. Double arrow indicates lasing transition and two arrows pointing upwards indicate ESA transitions to higher excited states in some low field material.

and d^7 configurations do not fit into this scheme and we will exclude them from our considerations. As shown in Fig. 2 and Tables I to III in all cases considered there are a few exchange split states of the lowest energy strong field configuration. The energies of those states depend only very weakly on the crystal field strength and transitions between them give sharp lines in emission and/or absorption (see Fig. 3). All are high-spin systems (the Hund rule is valid) and the ground state is $(t_{2g}^2)^3T_{1g}$ for d^2, $(t_{2g}^3)^4A_{2g}$ for d^3 and $(t_{2g}^6 e_g^2)^3A_{2g}$ for d^8. The energy differences

between the two lowest states of this configuration ΔE are:

$$\begin{aligned} \Delta E &= 2(3B + C) = 2K(\xi, \eta) \qquad \text{for } d^2, \\ \Delta E &= 3(3B + C) = 3K(\xi, \eta) \qquad \text{for } d^3, \\ \Delta E &= 2(4B + C) = 2K(u, v) \qquad \text{for } d^8, \end{aligned} \tag{18}$$

where $K(\xi, \eta)$ is an exchange integral calculated with two different base functions ξ and η of the t_{2g} representation, and $K(u, v)$ is an exchange integral calculated with two base functions u and v of the e_g representation spanned by d-functions. Since ΔE does not depend on the crystal field parameter 10 Dq, transition energies between states of the same configuration are independent of the ionic vibrations (which change the crystal field). Only transitions between states of different configurations do couple strongly to the lattice. Therefore intra-configurational transitions between the states of the lowest configuration do not provide broad bands in absorption or emission important for the performance of the flashlamp pumped tunable laser. In emission they may even be detrimental by providing a competing narrow band transition (like in ruby) making a tunable laser operation impossible. Also, since all of them, except the ground state, are of the different spin multiplicity, intra-configurational transitions are spin-forbidden. We conclude that only inter-configurational transitions between states of the same multiplicity can provide broad band transitions with relatively large oscillator strengths in absorption and reasonable stimulated emission cross sections important for the efficient operation of the laser although k-electron jumps, $t_{2g}^n e_g^m \longrightarrow t_{2g}^{n-k} e_g^{m+k}$, for $|k| \geq 2$ are forbidden as well. For all those reasons only high-spin states of the next configuration (10 Dq higher in energy) are of interest and are included in Tables I to III. We have also included the 20 Dq configuration high-spin state since it can participate in excited state absorption (ESA) transition from the 10 Dq configuration. In order to have a broad band operation the lowest energy state of this configuration has to be the first excited state. Therefore we formulate the low field condition:

$$\begin{aligned} 10Dq - 3B &\leq 2(3B + C) \qquad \text{for } d^2, \\ 10Dq &\leq 3(3B + C) \qquad \text{for } d^3, \\ 10Dq &\leq 2(4B + C) \qquad \text{for } d^8. \end{aligned} \tag{19}$$

illustrated in Fig. 3. Figure 3 shows absorption, luminescence excitation and luminescence spectra of Cr^{3+} in kyanite (for more details see [8]). Broad bands in absorption and luminescence excitation spectra correspond to spin-allowed intra-configurational transitions from the $^4A_{2g}$ ground state. Emission spectra are due to different sites characterized by different values of crystal field parameter 10 Dq, some complying with condition (19) and some not. It is interesting to note that relatively small change in 10 Dq value brings about a drastic change in appearance of the luminescence spectra, broad band being replaced by sharp lines, [8].

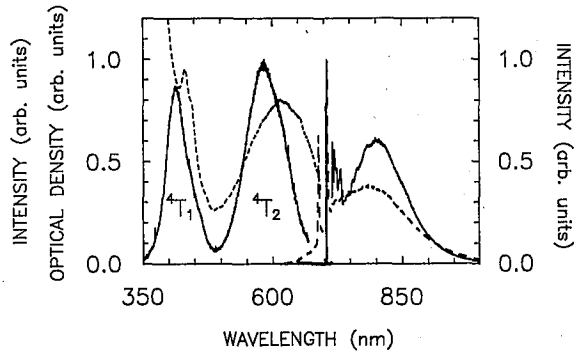

Fig. 3. Absorption, luminescence excitation and luminescence spectra of Cr^{3+} in kyanite. $^4T_2$ and $^4T_1$ indicate broad bands in absorption and luminescence excitation spectra due to transitions from the $^4A_2$ group state to appropriate states of the $10Dq$ strong field configuration. Solid line — luminescence excitation spectrum, dashed line — absorption spectrum. Emission spectra are complex, showing sharp lines due to intra-configurational transitions around 700 nm and broad band peaking about 800 nm coming from the inter-configurational transition. Solid line — steady state spectrum at 26 K, dashed line — steady state spectrum at 3000 K.

The next condition derives from the requirement that the ESA transitions should have the "gap" covering the emission band. Since for those transitions the ground state will be the lowest energy excited state, we are now interested in higher energy and the same multiplicity states (of any configuration). Taking into account the Stokes shift this condition can be formulated as follows:

$$\begin{aligned} &12B \leq 10Dq - 3B - 2S\hbar\omega \leq 10Dq, && \text{for } d^2, \\ &12B \leq 10Dq - 2S\hbar\omega \leq 10Dq + 3B, && \text{for } d^3, \\ &12B \leq 10Dq - 2S\hbar\omega \leq 10Dq + 3B, && \text{for } d^8. \end{aligned} \tag{20}$$

The lower limit transition ends up on the state of the same configuration, therefore we expect it to be relatively narrow. It turns out not to be true, [9]. The reason is, most likely, in significant coupling to lower symmetry modes shifting the equilibrium positions of the two adiabatic energy parabolas corresponding to relevant excited states, [9]. The high energy limit is of no significance for the operation of the laser.

In Fig. 4 we show the X–$10Dq$ diagram covering all materials activated with d^2, d^3 and d^8 ions. X and $10Dq$ are expressed in units of B. We define X as the energy of the transition between the ground state and the exchange split excited of the same configuration which, for low field materials, can often be easily estimated from the position of the characteristic Fano resonances showing up in the absorption spectrum, [10]. Also 10 Dq can be found from absorption

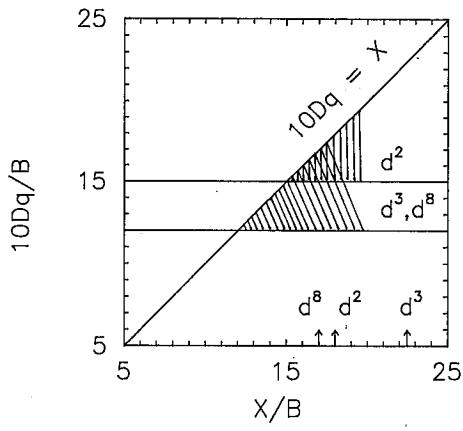

Fig. 4. X–$10Dq$ diagram for d^2, d^3 and d^8 systems. X is an exchange splitting energy, $10Dq$ — crystal field parameter. Equation $10Dq = X$ designates a line representing a low field condition (condition is fulfilled below the line), horizontal lines express the ESA "open window" condition (a condition for a given configuration is fulfilled above the appropriate line). In shadowed areas both conditions are fulfilled simultaneously. Arrows indicate values of X/B for appropriate configuration.

spectra, therefore both parameters can be evaluated experimentally and the point corresponding to the given material in the X–$10\ Dq$ diagram can easily be found. Since, approximately, $C = 4.5\ B$ [6], X for different configurations in units of B should be equal to:

$$\begin{aligned} &\text{for } d^2 \quad X = 15, \\ &\text{for } d^3 \quad X = 22.5, \text{ and} \\ &\text{for } d^8 \quad X = 17. \end{aligned} \tag{21}$$

The low field condition (19) can be rewritten as:

$$\begin{aligned} &\text{for } d^2 \quad 10Dq \leq X + 3 = X' \quad \text{and} \quad X' = 18 \\ &\text{for } d^3 \text{ and } d^8 \quad 10Dq \leq X. \end{aligned} \tag{22}$$

The ESA condition (20) (we omit the Stokes shift term) will read:

$$\begin{aligned} &\text{for } d^2 \quad 10Dq \geq 15 \\ &\text{for } d^3 \quad 10Dq \geq 12, \text{ and} \\ &\text{for } d^8 \quad 10Dq \geq 12. \end{aligned} \tag{23}$$

The low field condition (22) and the ESA condition (23) can be represented by straight lines in the X–$10Dq$ diagram, which define the useful range of $10Dq$ and X parameters shown by a shadowed area. The intersection of those lines defines a critical point (X_{cr}, $10Dq_{cr}$), which, in units of B, is (12, 12) for d^3 and d^8, and (15, 15) for d^2. It is interesting to note, that the critical point for Cr^{3+} lasers is only 12 while X is as large as 22.5. This means that the range of acceptable values of $10Dq$, which depends on the host, is 10.5, much larger than for d^2 or d^8 lasers (3 and 5 respectively). This explains why so many Cr^{3+} ion activated hosts were demonstrated to provide good tunable laser materials [2, 5].

5. Conclusions

The operation of the tunable solid-state laser based on TM ions of d^2, d^3 and d^8 configuration requires a specific ordering of excited of the ion. In low field materials, where crystal field parameter $10Dq$ is lower than the exchange splitting, the first excited state is due to the $10Dq$ strong field configuration, which provides a strongly lattice coupled transition characterized by a broad band in emission. This is essential for the tunability of the laser. However, there is a low energy limit imposed on the crystal field parameter $10Dq$ by a requirement of the "open window" in the excited state absorption coinciding with the emission band. This imposed a limit on the lowest $10Dq$. The range of acceptable $10Dq$ values is the largest for a d^3 configuration.

6. Acknowledgment

The author is grateful to Professor Alex Lempicki, who supervised the laser project at Boston University, for continuous support and many stimulating discussions.

References

[1] J.L. Emmett, W.F. Krupke, W.R. Sooy, *The Potential of High-Average-Power Solid State Lasers,* Lawrence Livermore National Laboratory, University of California, Livermore, CA 94550 1984 (UCRL — 53571, Distribution Category-21,22);
J.L Emmett, W.F Krupke, J.I. Davis, *IEEE J. Quantum Electron* **QE–20**, 591 (1984).

[2] J.A. Caird, in *Tunable Solid State Lasers II,* Eds. A.B. Budgor, L. Esterowitz, L.G. DeShazer, Springer-Verlag, New York 1986, p. 20.

[3] M.D. Sturge, *Solid State Phys.* **20**, 91 (1967).

[4] C.J. Donnelly, S.M. Healy, T.J. Glynn, G.F. Imbusch, G.P. Morgan, *J. Lumin.* **42**, 119 (1988);
A.J. Wojtowicz, M. Grinberg, A. Lempicki, submitted to *J. Lumin.*

[5] L.F. Johnson, R.E. Dietz, H.J. Guggenheim, *Phys. Rev. Lett.* **11**, 318 (1963);
J.C. Walling, H.P. Jenssen, R.C. Morris, E.W. O'Dell, O.G. Peterson *Optical Society of America Annual Meeting,* Nov. 1978;

J.C. Walling, O.G. Peterson, H.P. Jenssen, R.C. Morris, E.W. O'Dell, *IEEE J. Quantum Electron.* **QE–16**, 1302 (1980);

E.V. Zarikov, N.N. Ilichev, S.P. Kalitin, V.V. Laptev, A.A. Malyutin, V.V. Osiko, V.G. Ostroumov, P.P. Pashinin, A.M. Prokhorov, V.A. Smirnov, A.F. Unsykor, I.A. Shcherbakov, *Sov. J. Quantum Electron.* **13(a)**, 1274 (1983);

J. Drube, B. Struve, G. Huber, *Optics Commun.* **50**, 45 (1984);

U. Branch, U. Durr, *Opt. Lett.* **9**, 441 (1984);

H.P. Jenssen, S.T. Lai, *J. Opt. Soc. Am. B* **3**, 115 (1986);

P.F. Moulton, *J. Opt. Soc. Am. B* **3**, 125 (1986).

[6] S. Sugano, Y. Tanabe, H. Kamimura, *Multiplets of Transition-Metal Ions in Crystal,* Academic Press, New York 1970.

[7] J.S. Griffith, *The Theory of Transition Metal Ions,* (University Press, Cambridge 1961.

[8] A.J. Wojtowicz, A. Lempicki, *J. Lumin.* **46**, 271 (1990);

A.J. Wojtowicz, submitted to *J. Lumin.*.

[9] L.J. Andrews, S.M. Hitelman, M. Kokta, D. Gabbe, *J. Chem. Phys.* **84**, 5229 (1986).

[10] M.D. Sturge, H.J. Guggenheim, M.H.L. Price, *Phys. Rev. B* **2**, 2459 (1970);

A. Lempicki, L. Andrews, S.J. Nettel, B.C. McCollum, E.I. Solomon, *Phys. Rev. Lett.* **44**, 1234 (1980).